

The AURORA Survey: The Mass – Metallicity and Fundamental Metallicity Relations at $z \sim 2.3$ Based Purely on Direct T_e Metallicities

ALI AHMAD KHSTOVAN,¹ RYAN L. SANDERS,¹ ALICE E. SHAPLEY,² MICHAEL W. TOPPING,³ NAVEEN A. REDDY,⁴
 ALEX M. GARCIA,^{5,6,7} DANIELLE A. BERG,^{8,9} LEONARDO CLARKE,² FERGUS CULLEN,¹⁰ RICHARD S. ELLIS,¹¹
 N. M. FÖRSTER SCHREIBER,¹² KARL GLAZEBROOK,¹³ TUCKER JONES,¹⁴ DEREK J. MCLEOD,¹⁰ ANTHONY J. PAHL,¹⁵
 MAX PETTINI,¹⁶ AND PAUL TORREY^{5,6,7}

¹Department of Physics and Astronomy, University of Kentucky, 505 Rose Street, Lexington, KY 40506, USA

²Department of Physics & Astronomy, University of California, Los Angeles, 430 Portola Plaza, Los Angeles, CA 90095, USA

³Steward Observatory, University of Arizona, 933 N Cherry Avenue, Tucson, AZ 85721, USA

⁴Department of Physics & Astronomy, University of California, Riverside, 900 University Avenue, Riverside, CA 92521, USA

⁵Department of Astronomy, University of Virginia, 530 McCormick Road, Charlottesville, VA 22904

⁶Virginia Institute for Theoretical Astronomy, University of Virginia, Charlottesville, VA 22904, USA

⁷The NSF-Simons AI Institute for Cosmic Origins, USA

⁸Department of Astronomy, The University of Texas at Austin, 2515 Speedway, Stop C1400, Austin, TX 78712, USA

⁹Cosmic Frontier Center, The University of Texas at Austin, Austin, TX 78712, USA

¹⁰Institute for Astronomy, University of Edinburgh, Royal Observatory, Edinburgh, EH9 3HJ, UK

¹¹Department of Physics & Astronomy, University College London, Gower Street, London WC1E 6BT, UK

¹²Max-Planck-Institut für extraterrestrische Physik (MPE), Giessenbachstr.1, D-85748 Garching, Germany

¹³Centre for Astrophysics and Supercomputing, Swinburne University of Technology, P.O. Box 218, Hawthorn, VIC 3122, Australia

¹⁴Department of Physics and Astronomy, University of California Davis, 1 Shields Avenue, Davis, CA 95616, USA

¹⁵The Observatories of the Carnegie Institution for Science, 813 Santa Barbara Street, Pasadena, CA 91101, USA

¹⁶Institute of Astronomy, Madingley Road, Cambridge CB3 0HA, UK

ABSTRACT

We present new constraints on the Mass – Metallicity (MZR) and Fundamental Metallicity Relations (FMR) using a sample of 34 galaxies at $1.38 \leq z \leq 3.5$ (median $z = 2.28$). These galaxies have direct T_e measurements from [OIII]4363Å and/or [OII]7320,7331Å auroral emission lines detected with *JWST*/NIRSpec as part of the AURORA survey. The detection of both oxygen auroral lines allows for dual-zone direct T_e measurements and expands the dynamic range in $12 + \log(\text{O/H})$ (7.68 to 8.65 dex), stellar mass (10^8 to $10^{10.4} \text{ M}_\odot$), and star-formation rate (1 to $100 \text{ M}_\odot \text{ yr}^{-1}$) compared to previous direct T_e studies of the high-redshift MZR and FMR. We characterize the $z \sim 2$ MZR and find a slope of 0.27 ± 0.04 and normalization of $12 + \log(\text{O/H}) = 8.44 \pm 0.04$ at 10^{10} M_\odot with an intrinsic scatter of 0.10 dex, consistent with past strong-line MZR measurements. Comparisons with $z \sim 2$ predictions from six simulations reveal that none reproduce our observed MZR normalization evolution between $z \sim 0$ and $z \sim 2$. This discrepancy suggests current models do not fully capture the chemical enrichment and feedback processes occurring at cosmic noon. However, all 34 galaxies are on or above the star-forming main sequence such that our sample may be biased towards lower $12 + \log(\text{O/H})$ if the FMR persists at $z \sim 2$. Correcting for this selection effect would increase O/H by ≈ 0.1 dex at $10^{9.3} \text{ M}_\odot$ (the median mass of our sample) bringing our MZR into better agreement with that of TNG. Lastly, we find our $z \sim 2.3$ sample is consistent with the $z \sim 0$ FMR within 0.1 dex in O/H, indicating that the smooth secular mechanisms regulating chemical enrichment, star formation, stellar mass, and outflows were in place at cosmic noon.

Keywords: Galaxy evolution (594), Chemical abundances (224), Metallicity (1031), High-redshift galaxies (734), Emission line galaxies (459)

1. INTRODUCTION

Corresponding author: Ali Ahmad Khostovan
 akhostov@gmail.com

The metal content of the interstellar medium (ISM) provides a powerful tracer of the baryon cycle that regulates how galaxies grow over cosmic time. Gas-phase metallicities encode the cumulative effects of star formation, gas inflow, metal production, feedback-driven outflows, and recycling of enriched metals. Two key scaling relations between gas-phase metallicities ($12 + \log(\text{O/H})$) and galaxy properties encapsulate these processes: the Mass – Metallicity Relation (MZR; e.g., Tremonti et al. 2004) and the Fundamental Metallicity Relation (FMR; e.g., Mannucci et al. 2010), where the latter links star-formation rate (SFR), stellar mass, and gas-phase metallicity. Combined, these relations trace the underlying physical mechanisms that drive chemical enrichment, mix newly produced metals with accreted pristine gas, remove metals via outflows, and recycle enriched gas from the circumgalactic medium. Cosmic noon ($z \sim 1.5 - 3.5$) represents a key epoch where the Universe peaked in cosmic star-formation rate density and galaxies rapidly assembled their stellar mass (e.g., Madau & Dickinson 2014; Khostovan et al. 2015, 2016). Measuring the MZR and FMR during this epoch provides crucial insight into how galaxies chemically matured during the most active cosmic phase of galaxy assembly and how these relations evolved across cosmic time.

The ‘gold standard’ of metallicity measurements is the direct T_e method, which requires the detection of auroral emission lines such as [OIII]4363Å and [OII]7320,7331Å (Osterbrock & Ferland 2006). The ratio of these transitions relative to a bright counterpart from the same ion (i.e., [OIII]5007Å, [OII]3726,3729Å) is sensitive to the electron temperature which is used to convert emission-line flux ratios into ionic abundances through well-known atomic physics. However, auroral lines are notoriously difficult to observe beyond the local Universe with only a handful of pre-*JWST* studies constraining $12 + \log(\text{O/H})$ using this approach (e.g., Yuan & Kewley 2009; Christensen et al. 2012; Gburek et al. 2019, 2023; Sanders et al. 2016a, 2020, 2023b). A common alternative for inferring metallicities in star-forming galaxies at high redshift is to use strong-line calibrations that are based on either theoretical modeling (e.g., Kewley & Dopita 2002; Kewley et al. 2019) or empirical T_e -based data sets at low- z (e.g., Pettini & Pagel 2004; Marino et al. 2013; Curti et al. 2020).

Strong-line calibrations provide the added advantage of robust number statistics as they only require measurements of key emission lines that are easily detectable from ground-based observatories relative to auroral lines. These calibrations have enabled systematic investigations of both MZR and FMR at $z \sim 1.5 - 3.5$ (e.g., Erb et al. 2006; Cullen et al. 2014; Maier et al. 2014; Zahid et al. 2014; Sanders et al. 2015; Henry et al. 2021; Sanders et al. 2021; Topping et al. 2021; Revalska et al. 2024; Jain et al. 2025; Stanton et al.

2025). However, strong-line calibrations based on line ratios, such as N2 ([NII]6583Å/H α) and O3N2 ([OIII]5007Å/H β \times H α /[NII]6583Å), can suffer from an intrinsic scatter of $\sim 0.1 - 0.2$ dex (e.g., Pettini & Pagel 2004; Marino et al. 2013) and have systematic offsets of up to $\sim 0.5 - 1$ dex in inferred metallicity depending on which calibration is applied (see Kewley et al. 2019 for a review). This is further complicated by the fact that high-redshift galaxies differ in ISM conditions relative to $z \sim 0$ galaxies exhibiting harder ionizing spectra, higher ionization parameters, elevated electron densities, and more extreme excitation conditions (e.g., Steidel et al. 2014; Hayashi et al. 2015; Sanders et al. 2016b, 2023a; Khostovan et al. 2016, 2021, 2024, 2025; Isobe et al. 2023; Topping et al. 2025). Although past efforts have recalibrated strong-line relations using local analogs of cosmic noon galaxies (e.g., Curti et al. 2017; Bian et al. 2018; Pérez-Montero et al. 2021a; Nakajima et al. 2022), robust constraints on the MZR and FMR at high redshift require direct T_e measurements spanning a broad range of $12 + \log(\text{O/H})$, stellar mass, and SFR.

JWST has provided the needed sensitivity and wavelength coverage to not only detect the sought after [OIII]4363Å auroral line, but also several other auroral lines such as [OII]7320,7331Å, [SIII]6314Å, and [SII]4070Å at $z > 1.5$ (e.g., Rhoads et al. 2023; Curti et al. 2023; Nakajima et al. 2023; Sanders et al. 2023b, 2024; Laseter et al. 2024; Morishita et al. 2024). This enables multi-zone direct T_e metallicity measurements of the different ionization phases in HII regions. It also allows for a sizable number of auroral detections to recalibrate strong-line diagnostics using representative samples of cosmic noon galaxies (e.g., Nakajima et al. 2023; Laseter et al. 2024; Sanders et al. 2024, 2025; Chakraborty et al. 2025; Scholte et al. 2025).

In this Letter, we present direct T_e measurements of 34 cosmic noon galaxies at $1.38 \leq z \leq 3.50$ from the *JWST*/NIRSpec AURORA survey (Shapley et al. 2025). Direct T_e measurements are based on [OIII]4363Å and/or [OII]7320,7331Å auroral line detections, with 18/34 galaxies having both auroral lines detected. This represents one of the largest samples of direct T_e measurements at cosmic noon. We use this sample to constrain the MZR and FMR at $z \sim 2.3$ and compare our measurements with previous strong-line calibration measurements and predictions from a suite of simulations. The paper is structured as follows: §2 describes the AURORA survey and ancillary multi-wavelength photometric data; §3 highlights our methodologies for deriving direct metallicities, stellar masses, and SFRs; §4 describes our results showing our MZR and FMR measurements; §5 discusses how our results compare to past observations and simulations and the physical implications; and, §6 summarizes our main conclusions.

Throughout this paper, we assume a Kroupa (2001) initial mass function (IMF), Λ CDM ($H_0 = 70 \text{ km s}^{-1} \text{ Mpc}^{-1}$, $\Omega_m = 0.3$, $\Omega_\Lambda = 0.7$), and a solar oxygen abundance of $12 + \log(\text{O/H})_\odot = 8.69$ (Asplund et al. 2021)¹.

2. DATA

2.1. AURORA

The Assembly of Ultradeep Rest-optical Observations Revealing Astrophysics (AURORA) survey (PID: 1914; PIs: A. Shapley & R. L. Sanders) is a *JWST*/NIRSpec program consisting of two pointings: GOODS-N and COSMOS. We refer the reader to the survey paper for details on observing strategy, target selection, data reduction, and spectral extraction (Shapley et al. 2025). Each pointing is observed with G140M/F100LP (44204s), G235M/F170LP (28886s), and G395M/F290LP (15056s) allowing for contiguous spectral coverage from $1 - 5 \mu\text{m}$ (observer-frame) with $R \sim 1000$ and a sensitivity of $5 \times 10^{-19} \text{ erg s}^{-1} \text{ cm}^{-2}$ (3σ). A total of 36 primary targets ($1.38 < z < 4.41$; $z_{\text{med}} = 2.33$) were selected based on ground-based spectroscopy of the strong rest-optical lines that suggested the auroral [OIII]4363Å and/or [OII]7320,7331Å lines would be bright enough to detect in the AURORA integration times (12.3 h in G140M; 8.0 h in G235M; 4.2 h in G395M). Filler targets are also included and are described in detail in Shapley et al. (2025) with a total of 97 targets making up the full survey. Data reduction was done using the standard STScI *JWST* pipeline coupled with custom software routines (Shapley et al. 2025). 1D science and error spectra were extracted using the optimal technique (Horne 1986). Spectra were corrected for slit losses following Reddy et al. (2023a, 2025) and line fluxes were measured as described in Sanders et al. (2025).

2.2. Photometric Data

Ancillary photometric data the targets of this analysis were drawn from the DAWN *JWST* Archive (DJA; Brammer 2023; Valentino et al. 2023). In COSMOS, this imaging covers $0.4 - 5 \mu\text{m}$ in 15 filters: 7 *HST* and 8 *JWST*. *JWST*/NIRCam coverage is drawn from PRIMER (Donnan et al. 2024) and *HST* imaging is from several programs including COSMOS/ACS (Scoville et al. 2007), CANDELS (Grogin et al. 2011; Koekemoer et al. 2011; Nayyeri et al. 2017), UVCANDELS (Wang et al. 2025), and 3D-*HST* (Skelton et al. 2014). The imaging in GOODS-N consists of 9 *HST* and 11 *JWST* filters covering a wavelength range of $0.4 - 5 \mu\text{m}$. The *JWST* data is drawn from JADES (Eisenstein et al. 2023), CONGRESS (PID: 3577; PI: E. Egami), PANORAMIC (Williams et al.

2025), and FRESCO (Oesch et al. 2023). *HST* imaging is a combination of several key programs including CANDELS (Barro et al. 2019) and HDUV (Oesch et al. 2018).

3. METHODOLOGY

3.1. Sample selection

We selected all star-forming galaxies in AURORA at $z \leq 3.5$ with a signal-to-noise ratio ($S/N \geq 3$) detection of at least one of the auroral lines [OIII]4363Å and [OII]7320,7331Å, enabling robust direct metallicities. Quiescent galaxies and active galactic nuclei (selected from either broad H α features in the absence of broad forbidden lines, or else $\log_{10} [\text{NII}]/\text{H}\alpha > -0.3$) were excluded. This selection resulted in a sample of 34 star-forming galaxies at $1.38 \leq z \leq 3.8$ (median $z \approx 2.3$). In total, there are 26 [OIII]4363Å and 26 [OII]7320,7331Å detections, including 8 galaxies with only [OIII]4363Å, 8 galaxies with only [OII]7320,7331Å, and 18 galaxies with detections of both oxygen auroral lines allowing for T_e constraints of both the high- and low-ionization nebular zones. This sample covers ~ 1 dex in $12 + \log(\text{O/H})$ ranging from 7.68 to 8.65 dex and ~ 2.5 dex in stellar mass spanning $10^8 - 10^{10.5} \text{ M}_\odot$.

3.2. Direct T_e Metallicity

We refer the reader to Sanders et al. (2025) for details on how direct T_e metallicities and associated errors were derived for the AURORA targets. In brief, electron density (n_e), electron temperature (T_e), and dust reddening ($E(B - V)_{\text{gas}}$) were iteratively computed until convergence, using PyNeb (Luridiana et al. 2015) for all atomic and ionic calculations. All Balmer and Paschen H I lines detected at $S/N \geq 3$ were simultaneously fit to derive $E(B - V)_{\text{gas}}$, assuming the Cardelli et al. (1989) extinction curve, and all line fluxes were subsequently corrected for dust attenuation. The [SII]6716,6731Å doublet ratio was used to infer n_e if both [SII] lines were detected at $S/N \geq 3$. Otherwise, n_e was estimated from the relation $n_e = 40(1 + z)^{1.5} \text{ cm}^{-3}$ (Topping et al. 2025).² The high ($T_e(\text{O}^{++})$) and low ($T_e(\text{O}^+)$) ionization zone temperatures were computed from the [OIII]4363Å/5007Å and [OII]7320,7331Å/3726,3729Å line ratios, respectively. If either [OIII]4363Å or [OII]7320,7331Å did not have $S/N \geq 3$, then T_e for the corresponding ionization zone was estimated using the relation from Campbell et al. (1986), found to be consistent with dual-zone T_e constraints at $z \gtrsim 2$ in AURORA (Sanders et al. 2025) and other studies (Cataldi et al. 2025; Chakraborty et al. 2025). The ionic abun-

¹ This value is only used to express our derived O/H values in terms of a fraction of solar metallicity. Adopting the higher values of $12 + \log(\text{O/H})_\odot = 8.74 - 8.76$ recently found by some groups (Magg et al. 2022; Lodders et al. 2025) does not change our results.

² The density inferred from [SII] probes the low ionization zone which is appropriate for O $^+$, but may not reflect n_e of the high O $^{++}$ ionization zone. However, varying the assumed n_e from 10 to 5000 cm^{-3} negligibly changes the derived $T_e(\text{O}^{++})$ by < 1 percent.

dance ratios O^+/H and O^{++}/H were then inferred from the $[\text{OII}]3726,3729/\text{H}\beta$ and $[\text{OIII}]5007/\text{H}\beta$ ratios, respectively, using the T_e and n_e constraints. Total oxygen abundance was calculated as $\frac{\text{O}}{\text{H}} = \frac{\text{O}^+}{\text{H}} + \frac{\text{O}^{++}}{\text{H}}$.

3.3. Stellar Mass

The spectral energy distribution (SED) of each AURORA target was characterized using the multi-wavelength flux-calibrated imaging drawn from DJA (§2.2). Images in each filter were point spread function (PSF) matched by convolving with a 2D Gaussian kernel with $\text{FWHM} = \sqrt{\text{FWHM}_{\text{filter}}^2 - \text{FWHM}_{\text{F160W}}^2}$, where $\text{FWHM}_{\text{F160W}} = 0.19''$ represents the largest PSF among the filter set. Flux densities were derived from forced photometry measurements using `photutils` (Bradley et al. 2025), where Kron apertures were applied to the PSF-matched images in combination with the segmentation maps from DJA. We assumed a Kron scaling of 2.5 and minimum value for the unscaled Kron radius of 3.8 pixels. Photometric errors are based on the 1σ local background variation within the cutout, estimated by placing 1000 random apertures within the Kron area after masking out all sources using the segmentation maps.

We used the SED fitting code `Bagpipes` (Carnall et al. 2018) to estimate stellar masses assuming BPASS v2.2.1 (Stanway & Eldridge 2018) binary stellar population models and a Kroupa (2001) IMF with slopes -1.35 ($0.1 < M/\text{M}_\odot < 0.5$) and -2.35 ($0.5 < M < 300 \text{ M}_\odot$). Stellar metallicities could vary from $0.001 - 2 \text{ Z}_\odot$ but were limited by a Gaussian prior centered on $12 + \log(\text{O/H})$ measured from AURORA with a width equivalent to the 1σ uncertainties on $12 + \log(\text{O/H})$. We assumed a Calzetti et al. (2000) dust attenuation curve³ with $0 < A_V < 5$ mag and a nebular-to-stellar reddening ratio between 1 and 3, with uniform priors on both parameters.

Nebular emission contributions within the medium and broadband photometry were accounted for via photoionization models incorporated in `Bagpipes`. We computed custom nebular grids using `Cloudy` v17.03 (Ferland et al. 2017) assuming Nicholls et al. (2017) abundance pattern scaling, ionization parameters of $-4 \leq \log_{10} U \leq -1$ with 0.2 dex increments, and $n_e = 10, 50, 100, 500, 1000$, and 1500 cm^{-3} . For each target, the grid with density closest to the [SII]-derived n_e was adopted and the gas-phase metallicity was fixed to the value based on the derived direct T_e metallicity. Lastly, we assumed a non-parametric star-formation history with the continuity prior (Leja et al. 2019). We adopted 7 lookback time bins bounded by 0, 3, 10, 30, 100, 300, 1000, and 3000 Myr that are of equal size in logarithmic space (0.5

³ We find that assuming an SMC dust attenuation curve instead decreases the resulting stellar masses by 0.08 dex on average, a negligible shift relative to the statistical uncertainties of our MZR measurements (see §4.1).

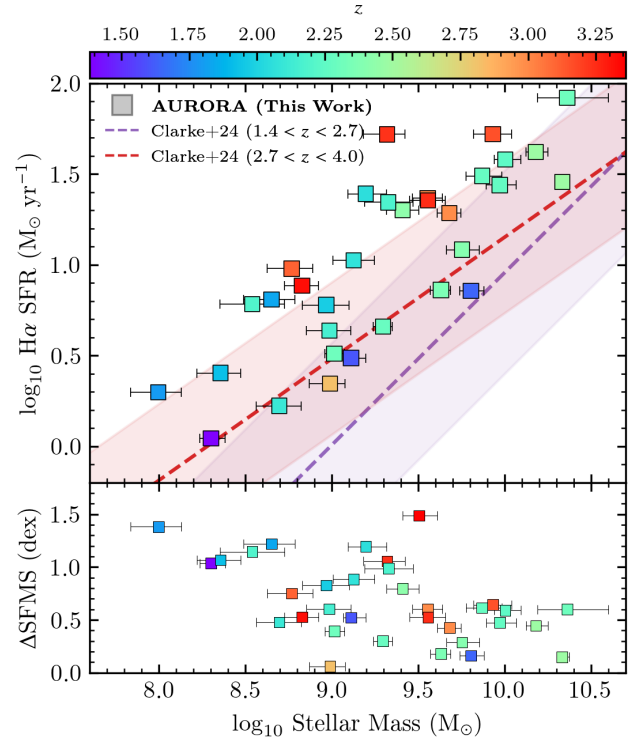


Figure 1. SFR vs. stellar mass for AURORA sources, shown in squares color-coded by redshift. Overlaid are the Clarke et al. (2024) star-forming main sequence relations based on $\text{SFR}(\text{H}\alpha)$. Offsets from the Clarke et al. (2024) relations are shown in the bottom panel. AURORA sources lie on and above the main sequence, reaching as high as 31 times the typical SFR at fixed mass.

dex), and a final bin extending to the age of the Universe at the spectroscopic redshift of the source.

3.4. Star-Formation Rates

SFRs were derived from the dust-corrected $\text{H}\alpha$ luminosity ($L_{\text{H}\alpha}$) using a metallicity-dependent conversion factor (Reddy et al. 2022, 2023b; Clarke et al. 2024) based on the relation presented in Sanders et al. (2025):

$$\frac{\text{SFR}}{\text{M}_\odot \text{ yr}^{-1}} = \left(C \frac{L_{\text{H}\alpha}}{\text{erg s}^{-1}} \right) 10^{0.89 \log_{10} Z + 0.14(\log_{10} Z)^2} \quad (1)$$

where $Z = 0.014 \times 10^{12+\log(\text{O/H})-8.69}$ is a function of the direct T_e metallicity and $C = 10^{-40.26}$. Figure 1 shows the SFRs and stellar masses of our sample compared to the $1.4 < z < 4$ star-forming main sequence relation from Clarke et al. (2024). All of our sources lie on or above this main-sequence parameterization, displaying offsets spanning 1.1 to 30.6 times (median: 4 times) the typical SFR at fixed stellar mass. This average offset above the main sequence is likely due to our requirement of detections of faint auroral $[\text{OIII}]4963\text{\AA}$ and/or $[\text{OII}]7320,7331\text{\AA}$ lines. Nebular lines are generally brighter with increasing SFR at fixed stellar

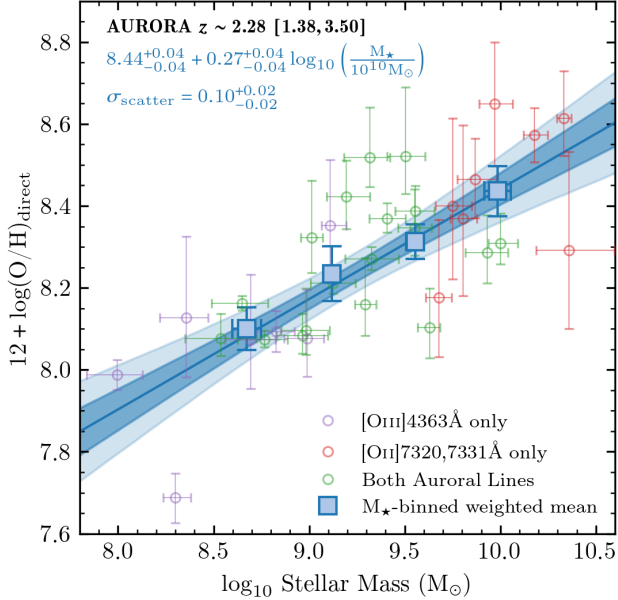


Figure 2. Mass metallicity relation for AURORA galaxies at $z \sim 2.3$ using only direct T_e metallicities. Open circles show individual galaxies color-coded based on whether [OIII]4363Å-only, [OII]7320,7331Å-only, or both oxygen auroral lines were detected. Our best-fit model (blue solid line) is shown along with the best-fit parameters and the darker (lighter) shading corresponds to the 1σ (2σ) confidence regions. Weighted mean values for equally populated stellar mass bins are shown for visualization purposes, but not used in fitting.

mass, but in the presence of an FMR higher-sSFR galaxies tend to have lower metallicities which is also associated with brighter auroral lines due to higher T_e values.

4. RESULTS

4.1. Mass - Metallicity Relation

Figure 2 shows the direct-method metallicities as a function of stellar mass for our AURORA sample of 34 galaxies. The high-mass, high-metallicity regime is dominated by objects with detections of [OII] $\lambda\lambda 7320,7331$ only, while the lowest-metallicity sources have [OIII] $\lambda 4363$ only. The use of both of these oxygen auroral lines in defining the sample allows for a wider dynamic range in both $12 + \log(O/H)$ and stellar mass, significantly improving direct MZR constraints at cosmic noon.

We fit a power-law model to the 34 individual galaxies in the sample, using:

$$12 + \log_{10}(O/H) = \gamma \log_{10} \left(\frac{M_{\star}}{10^{10} M_{\odot}} \right) + Z_{10} + \mathcal{N}(0, \sigma_{\text{MZR}}) \quad (2)$$

where Z_{10} is the value of $12 + \log(O/H)$ at $10^{10} M_{\odot}$ and γ represents the MZR slope. The last term takes into account the intrinsic scatter of O/H at fixed M_{\star} (σ_{MZR}). We use

emcee, a Monte Carlo Markov Chain (MCMC) python package (Foreman-Mackey et al. 2013), to sample the posterior distribution functions of each parameter. We adopt uniform priors for each parameter bounded in ranges of $7 < Z_{10} < 9$, $0 < \gamma < 0.5$, and $0.001 < \sigma_{\text{MZR}} < 0.5$. We consider 4000 steps with 64 walkers and burn-in $\sim 5 \times$ the maximum auto-correlation time (≈ 37 steps). The resulting best-fit parameters are taken to be the 50th percentile for each parameter, shown in Figure 2. For visualization purposes, we also display inverse-variance weighted means in equally-populated bins of stellar mass. The best-fit model has a slope of $\gamma = 0.27 \pm 0.04$ and a normalization of $12 + \log(O/H) = 8.44 \pm 0.04$ at $10^{10} M_{\odot}$, with an intrinsic scatter of 0.10 ± 0.02 dex.

4.2. Fundamental Metallicity Relation

The Fundamental Metallicity Relation represents the three-dimensional relation among SFR, stellar mass, and gas-phase metallicity. A simple representation of the FMR is a projection onto a two-dimensional $12 + \log(O/H) - \mu$ plane defined by $\mu = \log_{10} M_{\star} - \alpha \log_{10} \text{SFR}$, where the value of α minimizes the scatter in $12 + \log(O/H)$ at fixed μ and is thus dependent on how metallicities were derived in different studies (e.g., Mannucci et al. 2010; Andrews & Martini 2013; Curti et al. 2020). Our sample size with direct T_e metallicities is not statistically large enough to constrain α directly at $z \sim 2$. We instead investigate whether the $z \sim 2$ population is consistent with the FMR calibrated at $z \sim 0$ on average, comparing to the $z \sim 0$ parameterizations of Sanders et al. (2021) with $\alpha = 0.60$ and Curti et al. (2020) with $\alpha = 0.55$. The results of this comparison are shown in Figure 3. For the $z \sim 2$ AURORA sample, we find median offsets in O/H at fixed μ of $-0.058^{+0.106}_{-0.083}$ dex relative to the Sanders et al. (2021) FMR and $-0.070^{+0.107}_{-0.085}$ dex relative to that of Curti et al. (2020), factoring in the uncertainties of each individual $12 + \log(O/H)$ and μ value. Our sample selection considering both the auroral [OIII]4363Å and [OII]7320,7331Å lines again leads to a wider dynamic range in properties, extending the range of μ by ~ 0.5 dex compared to a sample selected based on [OIII]4363Å detection alone. The binned weighted means show a correlation between $12 + \log(O/H)$ and μ with a similar slope to what is seen at $z \sim 0$.

5. DISCUSSION

5.1. Comparison to Observations

We compare our best-fit direct T_e $z \sim 2$ MZR based purely on direct T_e metallicities to observational constraints from past studies at similar redshift in the left panel of Figure 4. We find that our direct MZR measurement is consistent within $\sim 1\sigma$ with past measurements at $z \sim 2$ that used either direct T_e (Sanders et al. 2020) or strong-line calibrations (Henry et al. 2021; Sanders et al. 2021; Revalski et al. 2024; Jain et al. 2025; Stanton et al. 2025). The

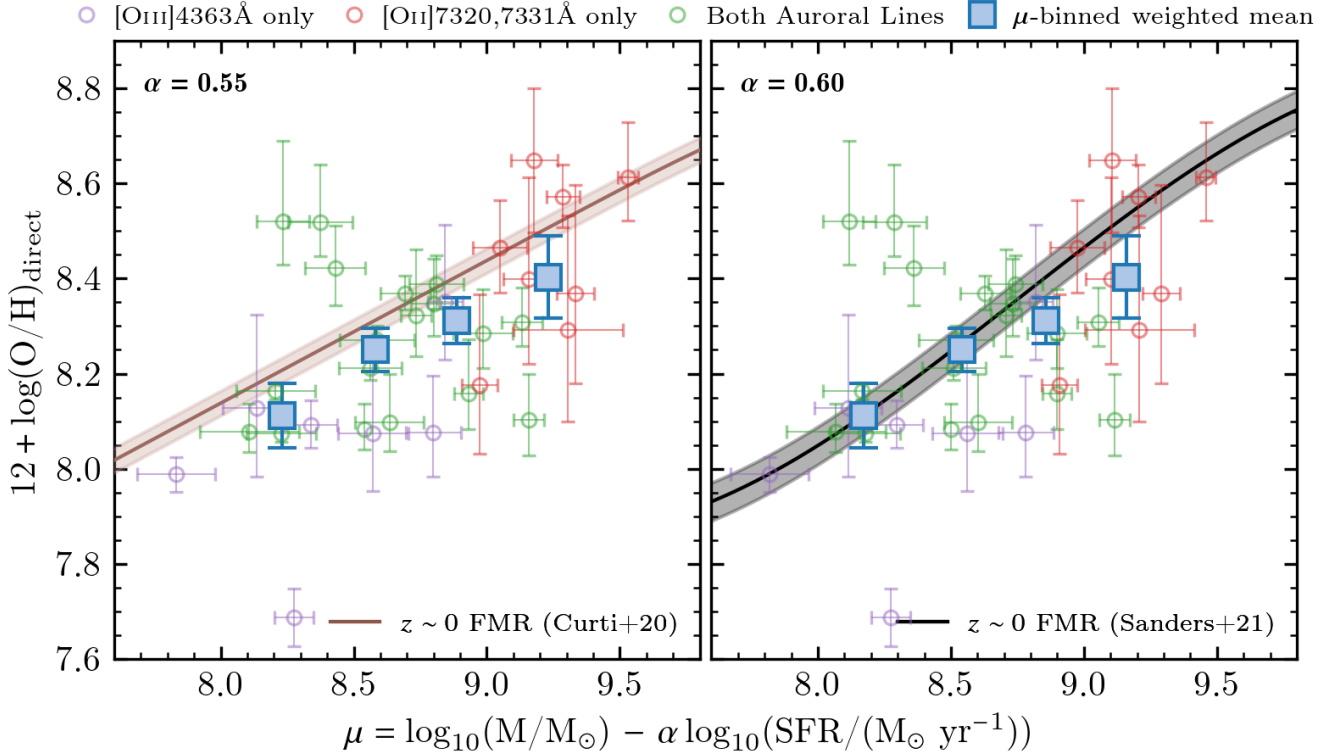


Figure 3. Fundamental Metallicity Relation with two different α that minimizes the scatter in $12 + \log(\text{O/H})$ at $z \sim 0$. Our measurements show how combining both [OIII] and [OII] auroral lines results in a ~ 1.5 dex coverage in μ from direct T_e measurements. We find our measurements are in strong agreement with the Sanders et al. (2021) FMR (right) with only a deviation at $\mu > 8.7$ although still within 1σ errors. The left panel shows the comparison with the Curti et al. (2020) FMR where we find agreement within 1σ but ~ 0.07 dex systematically lower $12 + \log(\text{O/H})$ at fixed μ which is within the typical uncertainties of strong-line calibrations. Overall, this suggests that the same physical processes regulating star formation, stellar mass build-up, and chemical enrichment at $z \sim 0$ is in place at cosmic noon.

Sanders et al. (2020) direct T_e MZR at $z \sim 2$ is based on direct metallicities of 18 galaxies at $z = 1.4 - 3.6$, derived from 7 [OIII]4363Å and 11 OIII]1663Å detections from ground-based spectroscopy. Our new T_e -based MZR represents a significant improvement over this past work, nearly doubling the sample size, achieving a much higher average S/N from space-based JWST observations, and is based entirely on rest-optical auroral lines ([OIII]4363Å and/or [OII]7320,7331Å) to avoid the strong dust reddening systematics plaguing the use of rest-UV OIII]1663Å. Consequently, the uncertainties on our slope and normalization constraints are $\approx 3\times$ smaller than in Sanders et al. (2020). Other attempts to characterize the MZR via pure direct T_e metallicities have been at higher redshifts and with lower precision, such as Chakraborty et al. (2025) who investigated the MZR with 42 galaxies at $z = 3 - 10$ yielding an uncertainty on the normalization of ≈ 0.2 dex in O/H at fixed M_\star .

However, our direct T_e sample is biased toward higher than average SFR at fixed stellar mass (Figure 1). If a FMR exists at $z \sim 2$, then a selection bias toward high SFR would introduce a corresponding bias toward low $12 + \log(\text{O/H})$, potentially leading to an underestimate of the true MZR normal-

ization. The magnitude of such a bias (and a corresponding correction factor) depends on the strength of the O/H-SFR anticorrelation at fixed stellar mass. Sanders et al. (2020) used the Andrews & Martini (2013) $z \sim 0$ SDSS sample to characterize this relation, finding $\Delta \log_{10} \text{O/H} \propto -0.29 \times \Delta \log_{10} \text{SFR}$, where these offsets are relative to the mean MZR and star-forming main sequence, respectively. Sanders et al. (2021) reported a shallower slope of -0.19 ± 0.04 for this relation based on a sample at $z \sim 2.3$, providing evidence that a FMR does exist at this redshift. In contrast, Korhonen Cuestas et al. (2025) recently found no evidence for a significant anti-correlation between O/H and SFR at fixed mass in a $z \sim 2$ sample. Observational studies are thus not in consensus regarding the strength of the secondary dependence of O/H on SFR, nor on the existence of an FMR at $z \sim 2$.

Our best-fit T_e -based MZR shown in Figure 4 may thus represent a lower limit on the actual $z \sim 2$ MZR. We test how a correction to our measured O/H values assuming the Sanders et al. (2021) relation of $\Delta \log_{10} \text{O/H} \propto -0.19 \times \Delta \log_{10} \text{SFR}$ would affect our derived $z \sim 2$ MZR, adopting the Speagle et al. (2014) star-forming main sequence relation for consistency with past work. Figure 4 shows this

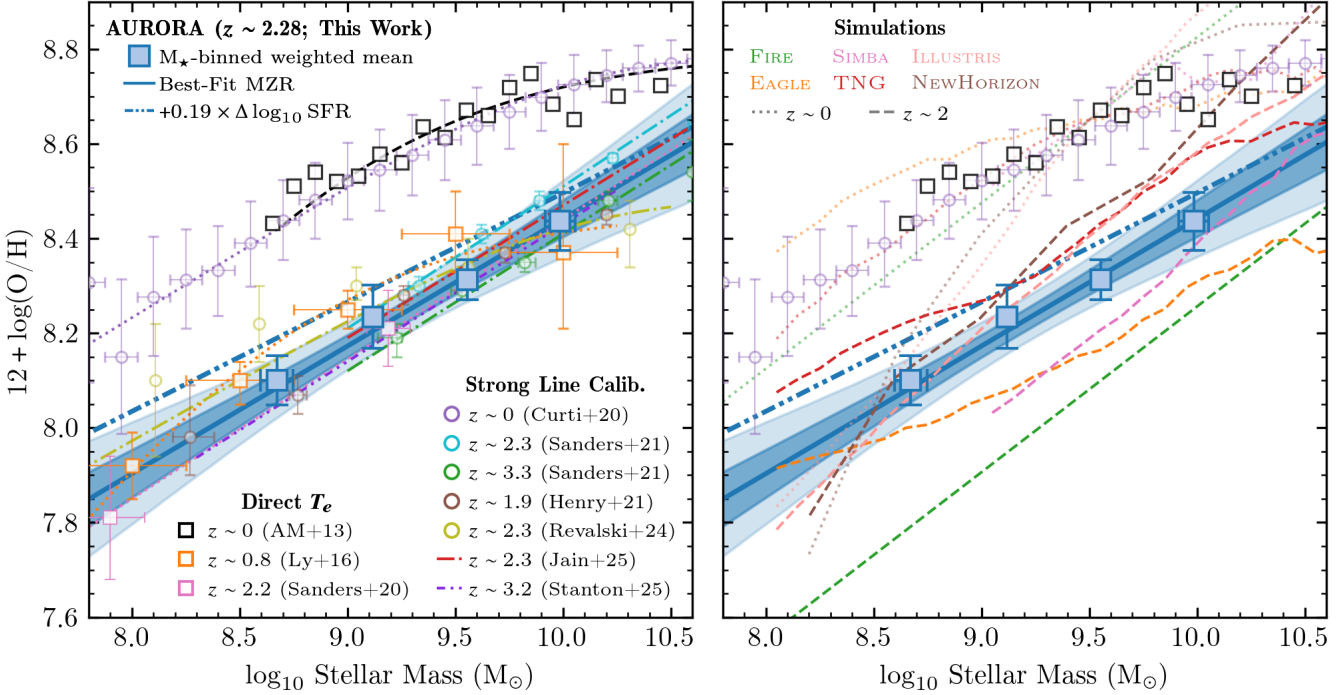


Figure 4. *Left:* Our best-fit Mass – Metallicity Relationship compared to past direct T_e (Curti et al. 2020; Ly et al. 2016; Sanders et al. 2020) and strong-line calibration (Henry et al. 2021; Sanders et al. 2021; Revalski et al. 2024; Jain et al. 2025; Stanton et al. 2025) MZR measurements. We find our MZR is in strong agreement with past MZR studies. We also include our $0.19 \times \Delta \log_{10} \text{SFR}$ corrected MZR that takes into account the bias towards high SFR, low mass systems. This MZR is found to result in increased $12 + \log(\text{O/H})$ towards low-mass relative to past MZR studies. However, the level of correction needed is uncertain. *Right:* Comparison of our MZR to different simulation predictions compiled by Garcia et al. (2025) including FIRE (Ma et al. 2016) and NewHorizon (Dubois et al. 2021). Only ILLUSTRISS and NewHorizon match in terms of normalization but have a steeper slope. All other simulations are found to have widely different normalizations but slopes consistent with our MZR measurement.

potential corrected MZR (blue dash dotted line), for which we find a slightly shallower slope and higher normalization ($\gamma = 0.23 \pm 0.05$, $12 + \log(\text{O/H}) = 8.50^{+0.05}_{-0.04}$ at 10^{10} M_\odot). This potential correction results in a slightly shallower MZR because the lowest-mass galaxies display the largest offsets from the main sequence (Fig. 1). However, this corrected MZR is $< 2\sigma$ consistent with our initial MZR constraints and thus does not represent a statistically significant shift overall. Given the current disagreement in the literature about the strength (or existence) of the anticorrelation between O/H and SFR at fixed mass at $z \sim 2$, further investigations are needed to understand whether our direct T_e MZR is substantially biased relative to the MZR of a more representative sample.

The agreement between our T_e -based MZR and past strong-line-based MZRs (e.g., Sanders et al. 2021; Jain et al. 2025) also highlights the reasonable performance of calibrations based on local analogs of high- z galaxies (e.g., Bian et al. 2018; Pérez-Montero et al. 2021b). Stanton et al. (2025) uses the Scholte et al. (2025) calibration (based on Laster et al. 2024), which is found to produce metallicities consistent with direct T_e measurements at $z \sim 2$ (Scholte et al.

2025). Henry et al. (2021) and Revalski et al. (2024) MZRs use the Curti et al. (2017) calibration, which is based on $z \sim 0$ direct T_e measurements from a representative (non-analog) SDSS sample. However, the difference in metallicity when applying ‘normal’ $z = 0$ vs. high-redshift analog strong-line calibrations to $z \sim 2$ samples is found to be $\approx 0.05 - 0.1$ dex (see Figure 11 of Sanders et al. 2021). Such shifts are only at the $1 - 2\sigma$ level relative to the MZR normalization uncertainty (0.04 dex) with our currently small direct T_e sample. We therefore conclude that the agreement between past MZR studies based on strong-line calibration and our new direct T_e MZR indicates that strong-line metallicity methods perform reasonably well for cosmic noon samples.

Figure 3 shows that our $z \sim 2$ sample does not display a large offset from the $z \sim 0$ FMR on average. For the Sanders et al. (2021) FMR ($\alpha = 0.60$), we find very close agreement at $\mu < 8.7$ and an average offset of $-0.12^{+0.13}_{-0.11}$ dex in O/H at $\mu > 8.7$, though the offset in the latter range is not statistically significant. Relative to the Curti et al. (2020) $z \sim 0$ FMR ($\alpha = 0.55$), the $z \sim 2$ sample displays small average offset in O/H at all values of μ : $-0.05^{+0.08}_{-0.06}$ dex and $-0.09^{+0.13}_{-0.11}$ dex at $\mu < 8.7$ and $\mu > 8.7$, respectively. In

both cases, we find that the typical offset in O/H at fixed μ is not statistically significant and suggests little FMR evolution ($\lesssim 0.1$ dex in O/H at fixed stellar mass and SFR) between $z \sim 0$ and $z \sim 2$, in agreement with past studies at this redshift based on strong-line metallicities (e.g., Kashino et al. 2017; Cresci et al. 2019; Sanders et al. 2021).

The non-evolution of the FMR and of the low-mass MZR power-law slope between $z = 0$ and $z \sim 2$ implies that the physical processes regulating metal enrichment, star formation activity, and stellar mass build-up at $z \sim 0$ were already in place at cosmic noon, and that $z \sim 2$ galaxy growth is dominated by smooth secular processes over this mass range. Using analytical chemical evolution models applied to strong-line MZR constraints, Sanders et al. (2021) showed that the mass-scaling of outflow metal loading factors does not evolve out to $z \sim 3$, and found that higher gas fractions and metal removal efficiencies at fixed mass with increasing redshift drive the decreasing MZR normalization. Given our close agreement with the strong-line MZR and FMR of Sanders et al. (2021), our results are consistent with the same physical picture in which feedback and metal-enriched outflows shape the MZR and regulate SFR at cosmic noon in the same manner as at $z \sim 0$. The emergence of such smooth secular growth processes are also consistent with the establishment of tight cold gas scaling relations and rotationally-supported disks at $z \sim 2-3$ (e.g., Tacconi et al. 2020; Förster Schreiber & Wuyts 2020, and references therein).

5.2. Comparison to Simulations

A direct one-to-one comparison between simulations and observations is difficult as each simulation makes distinct assumptions about stellar yields, feedback and outflow prescriptions, recycling of gas, and star-formation prescriptions, all of which can cause differences in absolute metallicity normalization. Studies based on simulations also vary in the form of metallicity that they report (e.g., weighting by mass or SFR, aperture size, stellar vs. gas-phase, star-forming vs. entire galaxy population), which may not be consistent with the metallicity probed by empirical direct T_e measurements that trace ionized gas in HII regions.

In order to mitigate these effects, we use the compilation of simulation results of Garcia et al. (2025) that provides MZR predictions from EAGLE, SIMBA, Illustris, and IllustrisTNG. For each simulation, Garcia et al. (2025) only selects ‘well-resolved’ central galaxies (> 100 star and > 500 gas particles), limited to galaxies that have specific SFR that is > -0.5 dex from the median specific SFR – stellar mass relationship in each simulation. This selection ensures that the simulated populations represent star-forming galaxies in order to make fairer comparison with observed galaxy samples used in MZR investigations. Gas-phase metallicities are defined as the mass-weighted metallicity of all star-

forming gas, which should trace similar physical regions to the ionized gas in H II regions. We also compare to the MZR predictions from FIRE (Ma et al. 2016) and NewHorizon (Dubois et al. 2021).

To account for the different absolute metallicity scales in each simulation, we normalize the metallicities in each simulation so that their $z \sim 0$ MZRs have the same metallicity at a stellar mass of $10^{9.5} M_\odot$ as the Curti et al. (2020) $z \sim 0$ observational MZR. We perform the normalization at a $10^{9.5} M_\odot$ as this corresponds to the highest limiting ‘well-resolved’ mass threshold among the simulation set, that of SIMBA (Garcia et al. 2025). This mass is also well-matched to the median mass of our $z \sim 2 T_e$ sample. The same normalization factor is then applied to the $z \sim 2$ MZR predictions, such that the relative metallicity evolution between $z \sim 0$ and $z \sim 2$ is preserved.

Figure 4 compares our observational direct T_e MZR to the $z \sim 2$ predictions from these simulations. We find that $z \sim 2$ MZR normalizations present in the simulations are not consistent with our observations. TNG, Illustris, and NewHorizon overestimate the $z \sim 2$ metallicities by ≈ 0.1 dex, while FIRE, EAGLE, and SIMBA fall lower than our observations by $0.1 - 0.2$ dex in O/H. Even at $z \sim 0$, we find that only TNG is in reasonable agreement with the observational Curti et al. (2020) and Andrews & Martini (2013) MZRs at all stellar masses, while the others have either steeper or shallower MZR slopes and thus diverge at low and high masses. FIRE, TNG, and EAGLE have consistent $z \sim 2$ MZR slopes with our direct T_e MZR, while Illustris, NewHorizon, and SIMBA have significantly steeper slopes.

Our results highlight that simulations have not been able to fully reproduce the observed MZR at cosmic noon and imply that changes to the feedback, gas, and/or star-formation physics in these models is needed to properly model the baryon and chemical enrichment cycles. Figure 4 further shows that the disagreement between simulations and observations extends even to $z \sim 0$ where, even after our rescaling, NewHorizon and Illustris significantly diverge from the observed MZR shape. The range of different MZR evolution predictions among these 6 simulations also demonstrates that robust observational metallicity constraints across a range of redshifts can meaningfully distinguish the fidelity of different galaxy formation models. However, as discussed above, our $z \sim 2$ direct T_e MZR may be biased low in $12 + \log(\text{O/H})$ at fixed stellar mass due to a selection bias toward high SFR. The left panel of Figure 4 shows how our best-fit MZR would change if we apply a correction based on the $z \sim 2$ FMR strength reported in Sanders et al. (2021), which would lead to a ≈ 0.1 dex increase in O/H at $10^{9.5} M_\odot$ that would bring our results into better agreement with Illustris, TNG, and NewHorizon. This systematic shift due to potential selection bias highlights how further progress is needed on the

observational side to improve the fidelity of comparisons to simulations.

6. CONCLUSIONS

In this Letter, we present new constraints on the mass metallicity relation and the evolution of the FMR at cosmic noon based purely on direct T_e metallicities, using a sample of 34 galaxies at $z = 1.4 - 3.5$ drawn from the AURORA Survey. Our results are as follows:

- a) Our sample is made up of 34 star-forming galaxies at $1.38 \leq z \leq 3.50$ ($z_{\text{median}} = 2.28$) with direct T_e metallicities. 18 of these sources having detections of both the [OIII]4363Å and [OII]7320,7331Å auroral lines. Of the remaining 16, there are 8 galaxies each with detections of [OIII]4363Å only or [OII]7320,7331Å only. This sample expands sample size and dynamic range in $12 + \log(\text{O/H})$, stellar mass, and SFR used in constraining MZR and FMR relative to previous direct T_e -based studies at high redshift.
- b) We find a best-fit MZR with slope of $\gamma = 0.27^{+0.04}_{-0.04}$, and a MZR normalization of $12 + \log(\text{O/H}) = 8.44^{+0.04}_{-0.04}$ dex at 10^{10} M_\odot , with an intrinsic scatter of 0.10 ± 0.02 dex in O/H. These values are generally consistent with past $z \sim 2 - 3$ strong-line MZR measurements.
- c) We compare to MZR predictions from 6 simulations and find that none of them reproduce our observed MZR normalization evolution between $z = 0$ and $z \sim 2$. Eagle, FIRE, and TNG display $z \sim 2$ MZR slopes consistent with our constraints, while Illustris, SIMBA, and NewHorizon have steeper slopes. These discrepancies highlight that current models do not fully reproduce the chemical enrichment and feedback processes.
- d) All 34 galaxies in our sample lie on or above the star-forming main sequence relation at $z \sim 2$, which may lead to an underestimate $12 + \log(\text{O/H})$ at fixed stellar mass on average relative to a representative population of galaxies. We demonstrate that adopting the SFR-dependent correction to our measured O/H values of $+0.19 \times \Delta \log_{10} \text{SFR}$ correction suggested by [Sanders et al. \(2021\)](#) can raise our MZR by ≈ 0.1 dex in O/H at $10^{9.5} \text{ M}_\odot$, bringing our MZR into better agreement with the TNG prediction in both slope, normalization, and evolution between $z \sim 0$ and $z \sim 2$. However, better constraints on the internal FMR strength (or its existence) among $z \sim 2$ galaxies is required to robustly determine the degree of correction required.
- e) Our direct T_e measurements are consistent on average with the $z \sim 0$ FMR parameterizations of [Curti et al.](#)

(2020) and [Sanders et al. \(2021\)](#) within 0.1 dex in O/H at fixed stellar mass and SFR. We find no statistically significant evidence for FMR evolution between $z = 0$ and $z \sim 2$.

- f) Our findings of little-to-no FMR evolution and MZR slope evolution between $z = 0$ and $z \sim 2$ based purely on direct T_e metallicities suggests that the mechanisms driving smooth secular chemical enrichment, star formation activity, stellar mass buildup, and metal-rich outflows were in place at cosmic noon.

JWST has provided the required sensitivity to robustly and efficiently investigate not only just the heavily sought after [OIII]4363Å line, but also other key auroral lines that allow for a multi-zone analysis of electron temperatures and robust ionic abundance measurements within the interstellar medium of galaxies at cosmic noon. Future *JWST* programs will expand on this work, increasing the sample sizes to improve direct T_e metallicity constraints on MZR and FMR evolution and gain valuable insights into the baryon cycle during the most active period of star formation in the Universe. These measurements will also provide important constraints to further develop our chemical enrichment and feedback prescriptions in large cosmological, hydrodynamical simulations.

ACKNOWLEDGEMENTS

This work is based on observations made with the NASA/ESA/CSA James Webb Space Telescope. The data were obtained from the Mikulski Archive for Space Telescopes at the Space Telescope Science Institute, which is operated by the Association of Universities for Research in Astronomy, Inc., under NASA contract NAS 5-03127 for *JWST*. These observations are associated with program JWST-GO-01914. The specific observations analyzed can be accessed via [DOI: 10.17909/hvne-7139](https://doi.org/10.17909/hvne-7139). Support for program JWST-GO-01914 was provided by NASA through a grant from the Space Telescope Science Institute, which is operated by the Association of Universities for Research in Astronomy, Inc., under NASA contract NAS 5-03127.

Some of the data products presented herein were retrieved from the Dawn *JWST* Archive (DJA). DJA is an initiative of the Cosmic Dawn Center (DAWN), which is funded by the Danish National Research Foundation under grant DNRF140.

This work is based on observations taken by the 3D-HST Treasury Program (GO 12177 and 12328) with the NASA/ESA HST, which is operated by the Association of Universities for Research in Astronomy, Inc., under NASA contract NAS5-26555.

Facilities: JWST (NIRSpec and NIRCam), HST (ACS and WFC3)

Software: `photutils` (Bradley et al. 2025), `astropy` (Astropy Collaboration et al. 2013, 2018, 2022), `numpy` (Harris et al. 2020) `Bagpipes` (Carnall et al. 2018), `Cloudy` (Ferland et al. 2017), `emcee` (Foreman-Mackey et al. 2013), `PyNeb` (Luridiana et al. 2015)

REFERENCES

Andrews, B. H., & Martini, P. 2013, *ApJ*, 765, 140, doi: [10.1088/0004-637X/765/2/140](https://doi.org/10.1088/0004-637X/765/2/140)

Asplund, M., Amarsi, A. M., & Grevesse, N. 2021, *A&A*, 653, A141, doi: [10.1051/0004-6361/202140445](https://doi.org/10.1051/0004-6361/202140445)

Astropy Collaboration, Robitaille, T. P., Tollerud, E. J., et al. 2013, *A&A*, 558, A33, doi: [10.1051/0004-6361/201322068](https://doi.org/10.1051/0004-6361/201322068)

Astropy Collaboration, Price-Whelan, A. M., Sipőcz, B. M., et al. 2018, *AJ*, 156, 123, doi: [10.3847/1538-3881/aabc4f](https://doi.org/10.3847/1538-3881/aabc4f)

Astropy Collaboration, Price-Whelan, A. M., Lim, P. L., et al. 2022, *ApJ*, 935, 167, doi: [10.3847/1538-4357/ac7c74](https://doi.org/10.3847/1538-4357/ac7c74)

Barro, G., Pérez-González, P. G., Cava, A., et al. 2019, *ApJS*, 243, 22, doi: [10.3847/1538-4365/ab23f2](https://doi.org/10.3847/1538-4365/ab23f2)

Bian, F., Kewley, L. J., & Dopita, M. A. 2018, *ApJ*, 859, 175, doi: [10.3847/1538-4357/aabd74](https://doi.org/10.3847/1538-4357/aabd74)

Bradley, L., Sipőcz, B., Robitaille, T., et al. 2025, `astropy/photutils`: 2.3.0, 2.3.0, Zenodo, doi: [10.5281/zenodo.17129028](https://doi.org/10.5281/zenodo.17129028)

Brammer, G. 2023, grizli, 1.9.11, Zenodo, doi: [10.5281/zenodo.8370018](https://doi.org/10.5281/zenodo.8370018)

Calzetti, D., Armus, L., Bohlin, R. C., et al. 2000, *ApJ*, 533, 682, doi: [10.1086/308692](https://doi.org/10.1086/308692)

Campbell, A., Terlevich, R., & Melnick, J. 1986, *MNRAS*, 223, 811, doi: [10.1093/mnras/223.4.811](https://doi.org/10.1093/mnras/223.4.811)

Cardelli, J. A., Clayton, G. C., & Mathis, J. S. 1989, *ApJ*, 345, 245, doi: [10.1086/167900](https://doi.org/10.1086/167900)

Carnall, A. C., McLure, R. J., Dunlop, J. S., & Davé, R. 2018, *MNRAS*, 480, 4379, doi: [10.1093/mnras/sty2169](https://doi.org/10.1093/mnras/sty2169)

Cataldi, E., Belfiore, F., Curti, M., et al. 2025, arXiv e-prints, arXiv:2504.03839, doi: [10.48550/arXiv.2504.03839](https://doi.org/10.48550/arXiv.2504.03839)

Chakraborty, P., Sarkar, A., Smith, R., et al. 2025, *ApJ*, 985, 24, doi: [10.3847/1538-4357/adc7b5](https://doi.org/10.3847/1538-4357/adc7b5)

Christensen, L., Laursen, P., Richard, J., et al. 2012, *MNRAS*, 427, 1973, doi: [10.1111/j.1365-2966.2012.22007.x](https://doi.org/10.1111/j.1365-2966.2012.22007.x)

Clarke, L., Shapley, A. E., Sanders, R. L., et al. 2024, *ApJ*, 977, 133, doi: [10.3847/1538-4357/ad8ba4](https://doi.org/10.3847/1538-4357/ad8ba4)

Cresci, G., Mannucci, F., & Curti, M. 2019, *A&A*, 627, A42, doi: [10.1051/0004-6361/201834637](https://doi.org/10.1051/0004-6361/201834637)

Cullen, F., Cirasuolo, M., McLure, R. J., Dunlop, J. S., & Bowler, R. A. A. 2014, *MNRAS*, 440, 2300, doi: [10.1093/mnras/stu443](https://doi.org/10.1093/mnras/stu443)

Curti, M., Cresci, G., Mannucci, F., et al. 2017, *MNRAS*, 465, 1384, doi: [10.1093/mnras/stw2766](https://doi.org/10.1093/mnras/stw2766)

Curti, M., Mannucci, F., Cresci, G., & Maiolino, R. 2020, *MNRAS*, 491, 944, doi: [10.1093/mnras/stz2910](https://doi.org/10.1093/mnras/stz2910)

Curti, M., D'Eugenio, F., Carniani, S., et al. 2023, *MNRAS*, 518, 425, doi: [10.1093/mnras/stac2737](https://doi.org/10.1093/mnras/stac2737)

Donnan, C. T., McLure, R. J., Dunlop, J. S., et al. 2024, *MNRAS*, 533, 3222, doi: [10.1093/mnras/stae2037](https://doi.org/10.1093/mnras/stae2037)

Dubois, Y., Beckmann, R., Bournaud, F., et al. 2021, *A&A*, 651, A109, doi: [10.1051/0004-6361/202039429](https://doi.org/10.1051/0004-6361/202039429)

Eisenstein, D. J., Willott, C., Alberts, S., et al. 2023, arXiv e-prints, arXiv:2306.02465, doi: [10.48550/arXiv.2306.02465](https://doi.org/10.48550/arXiv.2306.02465)

Erb, D. K., Shapley, A. E., Pettini, M., et al. 2006, *ApJ*, 644, 813, doi: [10.1086/503623](https://doi.org/10.1086/503623)

Ferland, G. J., Chatzikos, M., Guzmán, F., et al. 2017, *RMxAA*, 53, 385, doi: [10.48550/arXiv.1705.10877](https://doi.org/10.48550/arXiv.1705.10877)

Foreman-Mackey, D., Hogg, D. W., Lang, D., & Goodman, J. 2013, *PASP*, 125, 306, doi: [10.1086/670067](https://doi.org/10.1086/670067)

Förster Schreiber, N. M., & Wuyts, S. 2020, *ARA&A*, 58, 661, doi: [10.1146/annurev-astro-032620-021910](https://doi.org/10.1146/annurev-astro-032620-021910)

Garcia, A. M., Torrey, P., Ellison, S. L., et al. 2025, *MNRAS*, 536, 119, doi: [10.1093/mnras/stae2587](https://doi.org/10.1093/mnras/stae2587)

Gburek, T., Siana, B., Alavi, A., et al. 2023, *ApJ*, 948, 108, doi: [10.3847/1538-4357/abc153](https://doi.org/10.3847/1538-4357/abc153)

—. 2019, *ApJ*, 887, 168, doi: [10.3847/1538-4357/ab5713](https://doi.org/10.3847/1538-4357/ab5713)

Grogan, N. A., Kocevski, D. D., Faber, S. M., et al. 2011, *ApJS*, 197, 35, doi: [10.1088/0067-0049/197/2/35](https://doi.org/10.1088/0067-0049/197/2/35)

Harris, C. R., Millman, K. J., van der Walt, S. J., et al. 2020, *Nature*, 585, 357, doi: [10.1038/s41586-020-2649-2](https://doi.org/10.1038/s41586-020-2649-2)

Hayashi, M., Ly, C., Shimasaku, K., et al. 2015, *PASJ*, 67, 80, doi: [10.1093/pasj/psv041](https://doi.org/10.1093/pasj/psv041)

Henry, A., Rafelski, M., Sunquist, B., et al. 2021, *ApJ*, 919, 143, doi: [10.3847/1538-4357/ac1105](https://doi.org/10.3847/1538-4357/ac1105)

Horne, K. 1986, *PASP*, 98, 609, doi: [10.1086/131801](https://doi.org/10.1086/131801)

Isobe, Y., Ouchi, M., Nakajima, K., et al. 2023, *ApJ*, 956, 139, doi: [10.3847/1538-4357/acf376](https://doi.org/10.3847/1538-4357/acf376)

Jain, S., Sanders, R. L., Khostovan, A. A., et al. 2025, arXiv e-prints, arXiv:2508.18369, doi: [10.48550/arXiv.2508.18369](https://doi.org/10.48550/arXiv.2508.18369)

Kashino, D., Silverman, J. D., Sanders, D., et al. 2017, *ApJ*, 835, 88, doi: [10.3847/1538-4357/835/1/88](https://doi.org/10.3847/1538-4357/835/1/88)

Kewley, L. J., & Dopita, M. A. 2002, *ApJS*, 142, 35, doi: [10.1086/341326](https://doi.org/10.1086/341326)

Kewley, L. J., Nicholls, D. C., & Sutherland, R. S. 2019, *ARA&A*, 57, 511, doi: [10.1146/annurev-astro-081817-051832](https://doi.org/10.1146/annurev-astro-081817-051832)

Khostovan, A. A., Malhotra, S., Rhoads, J. E., et al. 2024, *MNRAS*, 535, 2903, doi: [10.1093/mnras/stae2395](https://doi.org/10.1093/mnras/stae2395)

Khostovan, A. A., Sobral, D., Mobasher, B., et al. 2015, MNRAS, 452, 3948, doi: [10.1093/mnras/stv1474](https://doi.org/10.1093/mnras/stv1474)

—. 2016, MNRAS, 463, 2363, doi: [10.1093/mnras/stw2174](https://doi.org/10.1093/mnras/stw2174)

Khostovan, A. A., Malhotra, S., Rhoads, J. E., et al. 2021, MNRAS, 503, 5115, doi: [10.1093/mnras/stab778](https://doi.org/10.1093/mnras/stab778)

Khostovan, A. A., Kartaltepe, J. S., Brinch, M., et al. 2025, ApJ, 994, 34, doi: [10.3847/1538-4357/ae0330](https://doi.org/10.3847/1538-4357/ae0330)

Koekemoer, A. M., Faber, S. M., Ferguson, H. C., et al. 2011, ApJS, 197, 36, doi: [10.1088/0067-0049/197/2/36](https://doi.org/10.1088/0067-0049/197/2/36)

Korhonen Cuestas, N. A., Strom, A. L., Miller, T. B., et al. 2025, ApJ, 984, 188, doi: [10.3847/1538-4357/adc5f7](https://doi.org/10.3847/1538-4357/adc5f7)

Kroupa, P. 2001, MNRAS, 322, 231, doi: [10.1046/j.1365-8711.2001.04022.x](https://doi.org/10.1046/j.1365-8711.2001.04022.x)

Laseter, I. H., Maseda, M. V., Curti, M., et al. 2024, A&A, 681, A70, doi: [10.1051/0004-6361/202347133](https://doi.org/10.1051/0004-6361/202347133)

Leja, J., Carnall, A. C., Johnson, B. D., Conroy, C., & Speagle, J. S. 2019, ApJ, 876, 3, doi: [10.3847/1538-4357/ab133c](https://doi.org/10.3847/1538-4357/ab133c)

Lodders, K., Bergemann, M., & Palme, H. 2025, SSRv, 221, 23, doi: [10.1007/s11214-025-01146-w](https://doi.org/10.1007/s11214-025-01146-w)

Luridiana, V., Morisset, C., & Shaw, R. A. 2015, A&A, 573, A42, doi: [10.1051/0004-6361/201323152](https://doi.org/10.1051/0004-6361/201323152)

Ly, C., Malkan, M. A., Rigby, J. R., & Nagao, T. 2016, ApJ, 828, 67, doi: [10.3847/0004-637X/828/2/67](https://doi.org/10.3847/0004-637X/828/2/67)

Ma, X., Hopkins, P. F., Faucher-Giguère, C.-A., et al. 2016, MNRAS, 456, 2140, doi: [10.1093/mnras/stv2659](https://doi.org/10.1093/mnras/stv2659)

Madau, P., & Dickinson, M. 2014, ARA&A, 52, 415, doi: [10.1146/annurev-astro-081811-125615](https://doi.org/10.1146/annurev-astro-081811-125615)

Magg, E., Bergemann, M., Serenelli, A., et al. 2022, A&A, 661, A140, doi: [10.1051/0004-6361/202142971](https://doi.org/10.1051/0004-6361/202142971)

Maier, C., Lilly, S. J., Ziegler, B. L., et al. 2014, ApJ, 792, 3, doi: [10.1088/0004-637X/792/1/3](https://doi.org/10.1088/0004-637X/792/1/3)

Mannucci, F., Cresci, G., Maiolino, R., Marconi, A., & Gnerucci, A. 2010, MNRAS, 408, 2115, doi: [10.1111/j.1365-2966.2010.17291.x](https://doi.org/10.1111/j.1365-2966.2010.17291.x)

Marino, R. A., Rosales-Ortega, F. F., Sánchez, S. F., et al. 2013, A&A, 559, A114, doi: [10.1051/0004-6361/201321956](https://doi.org/10.1051/0004-6361/201321956)

Morishita, T., Stiavelli, M., Grillo, C., et al. 2024, ApJ, 971, 43, doi: [10.3847/1538-4357/ad5290](https://doi.org/10.3847/1538-4357/ad5290)

Nakajima, K., Ouchi, M., Isobe, Y., et al. 2023, ApJS, 269, 33, doi: [10.3847/1538-4365/acd556](https://doi.org/10.3847/1538-4365/acd556)

Nakajima, K., Ouchi, M., Xu, Y., et al. 2022, ApJS, 262, 3, doi: [10.3847/1538-4365/ac7710](https://doi.org/10.3847/1538-4365/ac7710)

Nayyeri, H., Hemmati, S., Mobasher, B., et al. 2017, ApJS, 228, 7, doi: [10.3847/1538-4365/228/1/7](https://doi.org/10.3847/1538-4365/228/1/7)

Nicholls, D. C., Sutherland, R. S., Dopita, M. A., Kewley, L. J., & Groves, B. A. 2017, MNRAS, 466, 4403, doi: [10.1093/mnras/stw3235](https://doi.org/10.1093/mnras/stw3235)

Oesch, P. A., Montes, M., Reddy, N., et al. 2018, ApJS, 237, 12, doi: [10.3847/1538-4365/aacb30](https://doi.org/10.3847/1538-4365/aacb30)

Oesch, P. A., Brammer, G., Naidu, R. P., et al. 2023, MNRAS, 525, 2864, doi: [10.1093/mnras/stad2411](https://doi.org/10.1093/mnras/stad2411)

Osterbrock, D. E., & Ferland, G. J. 2006, Astrophysics of gaseous nebulae and active galactic nuclei

Pérez-Montero, E., Amorín, R., Sánchez Almeida, J., et al. 2021a, MNRAS, 504, 1237, doi: [10.1093/mnras/stab862](https://doi.org/10.1093/mnras/stab862)

—. 2021b, MNRAS, 504, 1237, doi: [10.1093/mnras/stab862](https://doi.org/10.1093/mnras/stab862)

Pettini, M., & Pagel, B. E. J. 2004, MNRAS, 348, L59, doi: [10.1111/j.1365-2966.2004.07591.x](https://doi.org/10.1111/j.1365-2966.2004.07591.x)

Reddy, N. A., Topping, M. W., Sanders, R. L., Shapley, A. E., & Brammer, G. 2023a, ApJ, 952, 167, doi: [10.3847/1538-4357/acd754](https://doi.org/10.3847/1538-4357/acd754)

—. 2023b, ApJ, 948, 83, doi: [10.3847/1538-4357/acc869](https://doi.org/10.3847/1538-4357/acc869)

Reddy, N. A., Topping, M. W., Shapley, A. E., et al. 2022, ApJ, 926, 31, doi: [10.3847/1538-4357/ac3b4c](https://doi.org/10.3847/1538-4357/ac3b4c)

Reddy, N. A., Shapley, A. E., Sanders, R. L., et al. 2025, arXiv e-prints, arXiv:2506.17396, doi: [10.48550/arXiv.2506.17396](https://doi.org/10.48550/arXiv.2506.17396)

Revalski, M., Rafelski, M., Henry, A., et al. 2024, ApJ, 966, 228, doi: [10.3847/1538-4357/ad382c](https://doi.org/10.3847/1538-4357/ad382c)

Rhoads, J. E., Wold, I. G. B., Harish, S., et al. 2023, ApJL, 942, L14, doi: [10.3847/2041-8213/acaaf](https://doi.org/10.3847/2041-8213/acaaf)

Sanders, R. L., Shapley, A. E., Topping, M. W., Reddy, N. A., & Brammer, G. B. 2023a, ApJ, 955, 54, doi: [10.3847/1538-4357/acedad](https://doi.org/10.3847/1538-4357/acedad)

—. 2024, ApJ, 962, 24, doi: [10.3847/1538-4357/ad15fc](https://doi.org/10.3847/1538-4357/ad15fc)

Sanders, R. L., Shapley, A. E., Kriek, M., et al. 2015, ApJ, 799, 138, doi: [10.1088/0004-637X/799/2/138](https://doi.org/10.1088/0004-637X/799/2/138)

—. 2016a, ApJL, 825, L23, doi: [10.3847/2041-8205/825/2/L23](https://doi.org/10.3847/2041-8205/825/2/L23)

—. 2016b, ApJ, 816, 23, doi: [10.3847/0004-637X/816/1/23](https://doi.org/10.3847/0004-637X/816/1/23)

Sanders, R. L., Shapley, A. E., Reddy, N. A., et al. 2020, MNRAS, 491, 1427, doi: [10.1093/mnras/stz3032](https://doi.org/10.1093/mnras/stz3032)

Sanders, R. L., Shapley, A. E., Jones, T., et al. 2021, ApJ, 914, 19, doi: [10.3847/1538-4357/abf4c1](https://doi.org/10.3847/1538-4357/abf4c1)

Sanders, R. L., Shapley, A. E., Clarke, L., et al. 2023b, ApJ, 943, 75, doi: [10.3847/1538-4357/aca9cc](https://doi.org/10.3847/1538-4357/aca9cc)

Sanders, R. L., Shapley, A. E., Topping, M. W., et al. 2025, arXiv e-prints, arXiv:2508.10099, doi: [10.48550/arXiv.2508.10099](https://doi.org/10.48550/arXiv.2508.10099)

Scholte, D., Cullen, F., Carnall, A. C., et al. 2025, MNRAS, 540, 1800, doi: [10.1093/mnras/staf834](https://doi.org/10.1093/mnras/staf834)

Scoville, N., Abraham, R. G., Aussel, H., et al. 2007, ApJS, 172, 38, doi: [10.1086/516580](https://doi.org/10.1086/516580)

Shapley, A. E., Sanders, R. L., Topping, M. W., et al. 2025, ApJ, 980, 242, doi: [10.3847/1538-4357/adad68](https://doi.org/10.3847/1538-4357/adad68)

Skelton, R. E., Whitaker, K. E., Momcheva, I. G., et al. 2014, ApJS, 214, 24, doi: [10.1088/0067-0049/214/2/24](https://doi.org/10.1088/0067-0049/214/2/24)

Speagle, J. S., Steinhardt, C. L., Capak, P. L., & Silverman, J. D. 2014, ApJS, 214, 15, doi: [10.1088/0067-0049/214/2/15](https://doi.org/10.1088/0067-0049/214/2/15)

Stanton, T. M., Cullen, F., Carnall, A. C., et al. 2025, arXiv e-prints, arXiv:2511.00705, doi: [10.48550/arXiv.2511.00705](https://doi.org/10.48550/arXiv.2511.00705)

Stanway, E. R., & Eldridge, J. J. 2018, MNRAS, 479, 75, doi: [10.1093/mnras/sty1353](https://doi.org/10.1093/mnras/sty1353)

Steidel, C. C., Rudie, G. C., Strom, A. L., et al. 2014, ApJ, 795, 165, doi: [10.1088/0004-637X/795/2/165](https://doi.org/10.1088/0004-637X/795/2/165)

Tacconi, L. J., Genzel, R., & Sternberg, A. 2020, ARA&A, 58, 157, doi: [10.1146/annurev-astro-082812-141034](https://doi.org/10.1146/annurev-astro-082812-141034)

Topping, M. W., Shapley, A. E., Sanders, R. L., et al. 2021, MNRAS, 506, 1237, doi: [10.1093/mnras/stab1793](https://doi.org/10.1093/mnras/stab1793)

Topping, M. W., Sanders, R. L., Shapley, A. E., et al. 2025, MNRAS, 541, 1707, doi: [10.1093/mnras/staf903](https://doi.org/10.1093/mnras/staf903)

Tremonti, C. A., Heckman, T. M., Kauffmann, G., et al. 2004, ApJ, 613, 898, doi: [10.1086/423264](https://doi.org/10.1086/423264)

Valentino, F., Brammer, G., Gould, K. M. L., et al. 2023, ApJ, 947, 20, doi: [10.3847/1538-4357/acbefa](https://doi.org/10.3847/1538-4357/acbefa)

Wang, X., Teplitz, H. I., Smith, B. M., et al. 2025, ApJ, 980, 74, doi: [10.3847/1538-4357/ada4ab](https://doi.org/10.3847/1538-4357/ada4ab)

Williams, C. C., Oesch, P. A., Weibel, A., et al. 2025, ApJ, 979, 140, doi: [10.3847/1538-4357/ad97bc](https://doi.org/10.3847/1538-4357/ad97bc)

Yuan, T.-T., & Kewley, L. J. 2009, ApJL, 699, L161, doi: [10.1088/0004-637X/699/2/L161](https://doi.org/10.1088/0004-637X/699/2/L161)

Zahid, H. J., Kashino, D., Silverman, J. D., et al. 2014, ApJ, 792, 75, doi: [10.1088/0004-637X/792/1/75](https://doi.org/10.1088/0004-637X/792/1/75)